Energy Tank-Based Policies for Robust Aerial Physical Interaction with Moving Objects

Conference Paper

Author(s):
Brunner, Maximilian; Giacomini, Livio; Siegwart, Roland Y.; Tognon, Marco (iD)

Energy Tank-Based Policies for Robust Aerial Physical Interaction with Moving Objects

Maximilian Brunner, Livio Giacomini, Roland Siegwart, and Marco Tognon

Abstract— **Although manipulation capabilities of aerial robots greatly improved in the last decade, only few works addressed the problem of aerial physical interaction with dynamic environments, proposing strongly model-based approaches. However, in real scenarios, modeling the environment with high accuracy is often impossible. In this work, we aim at developing a control framework for Omnidirectional Micro Aerial Vehicles (OMAVs) for reliable physical interaction tasks with articulated and movable objects in the presence of possibly unforeseen disturbances, and without relying on an accurate model of the environment. Inspired by previous applications of energy-based controllers for physical interaction, we propose a passivity-based impedance and wrench tracking controller in combination with a momentum-based wrench estimator. This is combined with an energy-tank framework to guarantee the stability of the system, while energy and power flow-based adaptation policies are deployed to enable safe interaction with any type of passive environment. The control framework provides formal guarantees of stability, which is validated in practice considering the challenging task of pushing a cart of unknown mass, moving on a surface of unknown friction, as well as subjected to unknown disturbances. For this scenario, we present, evaluate and discuss three different policies.**

I. INTRODUCTION

In the last decade, there has been a growing attention to the field of Aerial Physical Interaction (APhI) [1]. In an effort towards enhancing manipulation capabilities of aerial robots, the problem has been addressed from different aspects, including the design of new control methods and new platforms more suited for interaction tasks. Those solutions lead to a new generation of aerial manipulators based on fully actuated, multi-, and omnidirectional thrust vehicles [2], capable to generate forces and torques in 6 degrees of freedom (DOF), and equipped with interaction tools like rigid rods [3], and articulated arms [4].

However, performing aerial interaction is inherently difficult due to the change of the system dynamics during interaction. Generally, we can identify two types of physical interaction: i) the one with a *static* environment, and ii) the one with a *dynamic* environment.

So far the research community mostly addressed APhI with static environments where the objective is to maintain contact or deliver a specific interaction force between the aerial robot and a rigid structure, while possibly sliding along its surface. In this case the environment is passive and its state does not change. Most works rely on position controllers driving the platform equipped with a mechanically compliant tool onto a surface [5], or on impedance
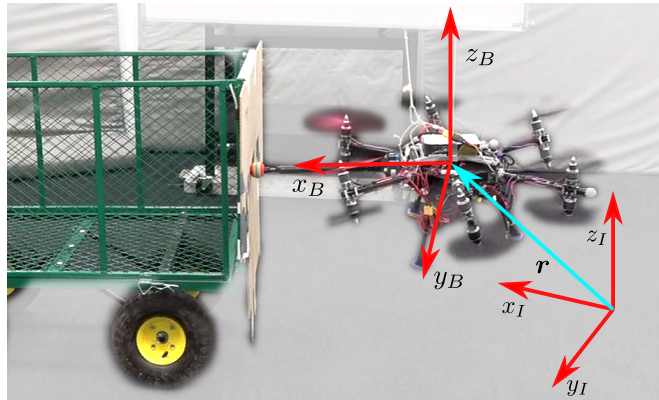
Fig. 1: An OMAV pushing a movable cart.

controllers [6], possibly also in combination with a force-tracking controller [7], [8]. Model-based solutions have been presented as well for push-and-slide operations [9], [10].

On the other hand, the less investigated interaction with dynamic environments (e.g. the aerial robot pushing a movable cart as illustrated in Fig. 1) implies additional challenges related to the change of state of the environment under the robot action, and vice versa. If the dynamics of the robot and the environment are perfectly known, a dynamic interaction task can theoretically be executed through a combination of accurate trajectory planning, state estimation of the entire system (robot and environment), and precise hybrid position-force control [11]. Along this line, recent works proposed both model-based and traditional motion-planning approaches. In [12] a Model Predictive Control (MPC) framework has been presented to open a hinged door, while in [13] the task of pushing a cart has been approached by dynamically updating the aerial robot position reference. While these approaches are able to tackle interaction tasks with dynamic environments in very structured conditions, no guarantees about their safety nor their robustness against model uncertainties and external disturbances can be made. In fact, in real scenarios, especially for aerial robotic applications, the state and physical characteristics of the environment are mostly unknown and unexpected disturbances may appear, drastically degrading performance eventually leading to the instability of the system.

To address the robustness issue during physical interaction, recent works proposed to study the system from an energetic perspective. In [14], the interaction is modeled employing the concept of power ports, considering the energy flow between interacting subsystems. When treating the system as an energy exchanging device, it is natural to use passivity as a stability criterion [15]. This principle has proven to be a

solid mathematical background in many areas such as in bilateral teleoperation [16], multi-robot coordination [17], [18], and physical human-robot interaction [19]. However, many control approaches and actions are not passive by design. Therefore, energy storage elements, also called *energy tanks*, were introduced in [20]. They allow to make non-passive actions passive using the stored energy s.t. the total internal energy of the system does not increase [21], [22].

Recently, this energy tank-based approach has been transferred to contact-based aerial inspection, where a similar setup was employed [23]. However, only interaction with static environments was investigated. On the contrary, we want to fully exploit the potential of passivity-based control methods to extend aerial physical interaction to dynamic environments ensuring stability and safety.

Using energy-based control techniques, additional safety features can be naturally deployed observing the energy exchange between sub-systems. In particular, the tank in- and outflow of energy, as well as the energy within the tank itself, can be exploited to implement high-level safety features. The work in [24] introduced the concept of *power valves* to limit the power exchange between the tank and the system for a ground manipulator.

In this work, we take inspiration from the works of [23] and [24] to develop a passivity-based control framework for robust APhI with dynamic environments, which can formally guarantee stability and safety. To this end, we design an impedance controller combined with a wrench tracking PI controller using a momentum-based wrench estimator considering an OMAV. We use an energy tank to restore the system's passivity and to guarantee stable interaction with any passive environment. The method does not require the knowledge of environment dynamics which can be time varying, as long as they remain passive.

While the energy tank ensures the overall systems passivity, we employ safety policies that are based on the energy stored within the tank, as well as on the magnitudes of the power flows between the tank and the system. These policies can adapt the control inputs to execute the interaction task while bounding the power flows to prevent potentially unsafe behaviors. To show the stability and safety properties of the proposed control framework, we challenge it with the complex task of pushing a cart of unknown mass under the presence of external disturbances and unknown friction conditions. In real experiments, we show that a standard interaction control method cannot provide enough stability and safety when physically interacting with dynamic environments under strong uncertainties and external disturbances. On the contrary, the introduced passivity-based method allows to meet this fundamental requirement. Additional practical considerations on different safety policies are provided as well.

II. MODELING

We use two frames for the derivation of the system dynamics: the inertial frame $\mathcal{F}_I = \{O_I, \boldsymbol{x}_I, \boldsymbol{y}_I, \boldsymbol{z}_I\}$ and the body-fixed frame $\mathcal{F}_B = \{O_B, \boldsymbol{x}_B, \boldsymbol{y}_B, \boldsymbol{z}_B\}$, where O_* represents the origin and $\boldsymbol{x}_*, \boldsymbol{y}_*, \boldsymbol{z}_*$ the primary axes of the frame. Let $\boldsymbol{R} \in \mathrm{SO}(3)$ be the rotation matrix representing

the rotation of $\mathcal{F}_B$ w.r.t. $\mathcal{F}_I$, and let $\boldsymbol{r} \in \mathbb{R}^3$ be the body position vector, given in $\mathcal{F}_I$. We define the body twist as the stacked angular and linear velocities, $\boldsymbol{\omega} \in \mathbb{R}^3$ and $\boldsymbol{v} \in \mathbb{R}^3$, respectively, both expressed in $\mathcal{F}_B$:

$$\boldsymbol{t} = \begin{bmatrix} \boldsymbol{\omega} \\ \boldsymbol{v} \end{bmatrix} \in \mathbb{R}^6. \qquad (1)$$

Then we define the momentum vector $\boldsymbol{p} \in \mathbb{R}^6$ as

$$\boldsymbol{p} = \boldsymbol{M}\boldsymbol{t}, \qquad (2)$$

where $\boldsymbol{M} = \mathrm{blkdiag}\,(\boldsymbol{J}, m\boldsymbol{I}_3) \in \mathbb{R}^{6\times 6}$ represents the generalized inertia tensor, containing the moment of inertia $\boldsymbol{J} \in \mathbb{R}^{3\times 3}$ and the system mass $m \in \mathbb{R}$.

Following the Newton-Euler approach we write the system dynamics as follows:

$$\underbrace{\begin{bmatrix} \boldsymbol{J} & \boldsymbol{0} \\ \boldsymbol{0} & m\boldsymbol{I}_3 \end{bmatrix}}_{\boldsymbol{M}} \underbrace{\begin{bmatrix} \dot{\boldsymbol{\omega}} \\ \dot{\boldsymbol{v}} \end{bmatrix}}_{\dot{\boldsymbol{t}}} = \underbrace{\begin{bmatrix} \boldsymbol{J}\,[\boldsymbol{\omega}]_\times & \boldsymbol{0} \\ \boldsymbol{0} & -m\,[\boldsymbol{\omega}]_\times \end{bmatrix}}_{\boldsymbol{C}} \begin{bmatrix} \boldsymbol{\omega} \\ \boldsymbol{v} \end{bmatrix}$$
$$+ \boldsymbol{w}_c + \boldsymbol{w}_g + \boldsymbol{w}_{ext}, \quad (3)$$

where[1] $\boldsymbol{w}_{ext} = \boldsymbol{w}_{dist} + \boldsymbol{w}_{int}$ comprises both disturbance and interaction wrenches defined by $\boldsymbol{w}_{dist} \in \mathbb{R}^6$ and $\boldsymbol{w}_{int} \in \mathbb{R}^6$, respectively; $\boldsymbol{w}_g \in \mathbb{R}^6$ represents the gravity force; and $\boldsymbol{w}_c \in \mathbb{R}^6$ the commanded wrench produced by the actuators.

III. INTERACTION CONTROL

Considering an OMAV in physical interaction, we employ an interaction control framework composed of an impedance controller combined with a wrench tracking PI controller using a momentum-based wrench estimator. In this section, we report the main derivations and the relative analysis of stability. As shown in [23], it turns out that such controller cannot guarantee the passivity of the system. In the following sections we shall then show how to guarantee passivity and add an extra safety layer.

A. Axis-Selective Impedance controller

Similar to [25] we introduce an Axis-Selective Impedance Control (ASIC). This gives us the advantage to set the desired virtual mass and inertia of the platform for each axis individually, combined in the desired generalized inertia tensor, $\boldsymbol{M}_d \in \mathbb{R}^{6\times 6}$.

We employ a momentum-based wrench observer to estimate the total external wrench acting on the platform, given by $\hat{\boldsymbol{w}}_{ext} = \begin{bmatrix} \hat{\boldsymbol{f}}_{ext}^\top & \hat{\boldsymbol{\tau}}_{ext}^\top \end{bmatrix}^\top \in \mathbb{R}^6$.

The impedance control law is then given by

$$\boldsymbol{w}_{c,imp} = \underbrace{\left(\boldsymbol{M}\boldsymbol{M}_d^{-1} - \boldsymbol{I}_6\right)}_{\bar{M}} \hat{\boldsymbol{w}}_{ext} - \boldsymbol{M}\boldsymbol{M}_d^{-1}\left(\boldsymbol{K}_d \boldsymbol{t} + \boldsymbol{K}_p \boldsymbol{e}\right)$$
$$- \boldsymbol{C}\boldsymbol{t} - \boldsymbol{w}_g$$
$$= \bar{\boldsymbol{M}}\hat{\boldsymbol{w}}_{ext} - \left(\bar{\boldsymbol{K}}_d \boldsymbol{t} + \bar{\boldsymbol{K}}_p \boldsymbol{e}\right) - \boldsymbol{C}\boldsymbol{t} - \boldsymbol{w}_g,$$
$$(4)$$

---

[1]The symbol $[\cdot]_\times : \mathbb{R}^3 \to \mathfrak{so}(3)$ represents the symmetric-skew operator such that, given two vector $\boldsymbol{y}, \boldsymbol{x} \in \mathbb{R}^3$, $[\boldsymbol{y}]_\times \, \boldsymbol{x} = \boldsymbol{y} \times \boldsymbol{x}$.
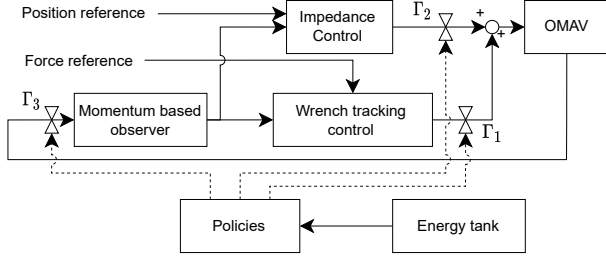
Fig. 2: Control block diagram including the valves which can scale the individual inputs.

with $\boldsymbol{K}_d, \boldsymbol{K}_p \in \mathbb{R}^{6 \times 6}_{>0}$, $\bar{\boldsymbol{K}}_d = \boldsymbol{M} \boldsymbol{M}_d^{-1} \boldsymbol{K}_d$ and $\bar{\boldsymbol{K}}_p = \boldsymbol{M} \boldsymbol{M}_d^{-1} \boldsymbol{K}_p$. The error vector $\boldsymbol{e} = \begin{bmatrix} \boldsymbol{e}_{rot}^\top & \boldsymbol{e}_{lin}^\top \end{bmatrix}^\top \in \mathbb{R}^6$ is composed of the angular and linear error, represented by

$$\boldsymbol{e}_{rot} = \frac{1}{2} \left(\boldsymbol{R}_d^\top \boldsymbol{R} - \boldsymbol{R}^\top \boldsymbol{R}_d \right)^\vee \tag{5a}$$

$$\boldsymbol{e}_{lin} = \boldsymbol{r} - \boldsymbol{r}_d, \tag{5b}$$

where[2] $\boldsymbol{R}_d \in \mathrm{SO}(3)$ represents the reference attitude and $\boldsymbol{r}_d \in \mathbb{R}^3$ the reference position of the platform. The gain matrices are composed from their linear and angular parts, i.e. $\boldsymbol{K}_p = \mathrm{blkdiag}\left(\boldsymbol{K}_{p,rot}, \boldsymbol{K}_{p,lin} \right)$ and $\boldsymbol{K}_d = \mathrm{blkdiag}\left(\boldsymbol{K}_{d,rot}, \boldsymbol{K}_{d,lin} \right)$, with $\boldsymbol{K}_{p,rot}, \boldsymbol{K}_{p,lin}, \boldsymbol{K}_{d,rot}, \boldsymbol{K}_{d,lin} \in \mathbb{R}^{3 \times 3}$. Combining (3), (4), and assuming $\boldsymbol{w}_{ext} = \hat{\boldsymbol{w}}_{ext}$, we obtain the closed loop dynamics:

$$\boldsymbol{M}_d \dot{\boldsymbol{t}} = -\boldsymbol{K}_d \boldsymbol{t} - \boldsymbol{K}_p \boldsymbol{e} + \boldsymbol{w}_{ext}. \tag{6}$$

B. Momentum based observer

The momentum based observer dynamics are [26]:

$$\hat{\boldsymbol{w}}_{ext} = \boldsymbol{K}_o(\boldsymbol{p} - \hat{\boldsymbol{p}}) \tag{7}$$

$$\dot{\hat{\boldsymbol{p}}} = \boldsymbol{C}\boldsymbol{t} + \boldsymbol{w}_g + \boldsymbol{w}_c + \boldsymbol{K}_o(\boldsymbol{p} - \hat{\boldsymbol{p}}), \tag{8}$$

where $\boldsymbol{K}_o \in \mathbb{R}^{6 \times 6}$ is the observer gain matrix. It follows that the wrench estimate tracks the true external wrench through a first order lowpass filter:

$$\dot{\hat{\boldsymbol{w}}}_{ext} = \boldsymbol{K}_o(\boldsymbol{w}_{ext} - \hat{\boldsymbol{w}}_{ext}). \tag{9}$$

C. Wrench tracking controller

In addition to the impedance controller we introduce a wrench tracking controller based on a PI law:

$$\boldsymbol{w}_{c,tr} = \boldsymbol{K}_{p,tr} \boldsymbol{w}_{int,e} + \boldsymbol{K}_{i,tr} \int \boldsymbol{w}_{int,e} dt \tag{10}$$

$$\boldsymbol{w}_{int,e} = \hat{\boldsymbol{w}}_{int} - \boldsymbol{w}_{int,d}, \tag{11}$$

with $\boldsymbol{K}_{p,tr}, \boldsymbol{K}_{i,tr} \in \mathbb{R}^{6 \times 6}$ being the proportional and integral controller gains, respectively. The estimated interaction wrench is composed of the external force estimate and zero torque, i.e. $\hat{\boldsymbol{w}}_{int} = \begin{bmatrix} \hat{\boldsymbol{f}}_{ext}^\top & \boldsymbol{0}_3 \end{bmatrix}^\top$.

We can then write the total control command $\boldsymbol{w}_c$ as

$$\boldsymbol{w}_c = \boldsymbol{w}_{c,imp} + \boldsymbol{w}_{c,tr}. \tag{12}$$

Figure 2 shows the control block diagram of the combined impedance and wrench tracking controller.

[2]The *vee*-map $(\cdot)^\vee : \mathfrak{so}(3) \to \mathbb{R}^3$ is the inverse of the skew-symmetric operator $[\cdot]_\times : \mathbb{R}^3 \to \mathfrak{so}(3)$.

D. Passivity analysis

We now analyze the stability of the system. In particular, we verify the passivity property considering the closed-loop system energy as storage function, $\mathcal{H}_{cl}$. The latter is defined as the sum of the kinetic energy of the platform $\mathcal{H}_{kin}$, the spring energy given by the impedance controller $\mathcal{H}_{spr}$, and the observer energy $\mathcal{H}_{obs}$:

$$\mathcal{H}_{cl} = \mathcal{H}_{kin} + \mathcal{H}_{spr} + \mathcal{H}_{obs}, \tag{13}$$

where

$$\mathcal{H}_{kin} = \frac{1}{2} \boldsymbol{p}^\top \boldsymbol{M}^{-1} \boldsymbol{p} = \frac{1}{2} \boldsymbol{t}^\top \boldsymbol{M} \boldsymbol{t} \tag{14a}$$

$$\mathcal{H}_{spr} = \frac{1}{2} \boldsymbol{e}_{lin}^\top \boldsymbol{K}_{p,lin} \boldsymbol{e}_{lin} + \frac{1}{2} \mathrm{tr}\left(\boldsymbol{K}_{p,rot}(\boldsymbol{I}_3 - \boldsymbol{R}_d^\top \boldsymbol{R}) \right) \tag{14b}$$

$$\mathcal{H}_{obs} = \frac{1}{2} \hat{\boldsymbol{p}}^\top \boldsymbol{K}_o \hat{\boldsymbol{p}}. \tag{14c}$$

By definition, the closed-loop system is said to be passive w.r.t. the input-output pair $(\boldsymbol{t}, \boldsymbol{w}_{ext})$ (the power port which acts between the platform and its environment), if the following inequality holds [15]:

$$\dot{\mathcal{H}}_{cl} \le \boldsymbol{t}^\top \boldsymbol{w}_{ext}. \tag{15}$$

Following similar steps as in [23], the time derivative of $\mathcal{H}_{cl}$ results in

$$\dot{\mathcal{H}}_{cl} = -\underbrace{\boldsymbol{t}^\top \bar{\boldsymbol{K}}_d \boldsymbol{t}}_{d_1} - \underbrace{\hat{\boldsymbol{p}}^\top \boldsymbol{K}_o^\top \boldsymbol{K}_o \hat{\boldsymbol{p}}}_{d_2}$$
$$+ \boldsymbol{t}^\top \boldsymbol{w}_{ext} + \underbrace{\boldsymbol{t}^\top}_{\boldsymbol{y}_1} \underbrace{\boldsymbol{w}_{c,tr}}_{\boldsymbol{\omega}_1} + \underbrace{\boldsymbol{t}^\top}_{\boldsymbol{y}_2} \underbrace{\bar{\boldsymbol{M}} \hat{\boldsymbol{w}}_{ext}}_{\boldsymbol{\omega}_2} \tag{16}$$
$$+ \underbrace{\hat{\boldsymbol{p}}^\top \boldsymbol{K}_o^\top}_{\boldsymbol{y}_3} \underbrace{(\boldsymbol{C}\boldsymbol{t} + \boldsymbol{w}_g + \boldsymbol{w}_c + \boldsymbol{K}_o \boldsymbol{p})}_{\boldsymbol{\omega}_3 := \dot{\hat{\boldsymbol{p}}} + \boldsymbol{K}_o \hat{\boldsymbol{p}}},$$

where $p_i := \boldsymbol{y}_i^\top \boldsymbol{\omega}_i$, $i \in \{1, 2, 3\}$ are the potentially passivity-violating power flows, since their signs are a priori undefined.

Analyzing (16), we can identify two damping terms, d_1 and d_2 which represent energy flowing out of the system. Conversely, the last three terms in (16) can be positive. As (15) can be violated, passivity cannot be always guaranteed. In order to ensure an overall passivity of the closed loop system, we extend the system dynamics with a virtual energy tank presented in the next section.

IV. ENERGY TANK

This virtual tank works as a energy reservoir that can be filled with the energy dissipated by damping terms and drained by the terms that can add energy to the system to compensate for them in the total energy balance. By designing the tank in- and outflows properly, we can achieve a cancellation of the passivity-violating terms in the total closed-loop dynamics.

We analyze (16) to identify the following power flows that can lead to a non-passive system:

- $p_1 = \boldsymbol{t}^\top \boldsymbol{w}_{c,tr}$, coming from wrench tracking commands;
- $p_2 = \boldsymbol{t}^\top \bar{\boldsymbol{M}} \hat{\boldsymbol{w}}_{ext}$, coming from components of the impedance controller;

- $p_3 = \hat{\boldsymbol{p}}^\top \boldsymbol{K}_o^\top \boldsymbol{\omega}_3$, coming from the wrench observer.

We then define the energy tank state as $x_t(t) \in \mathbb{R}$ and the tank energy as $\mathcal{H}_t = \frac{1}{2}x_t^2$. In order to constrain the available energy in the tank, we introduce a lower and an upper bound, $\mathcal{H}_t^-$ and $\mathcal{H}_t^+$, respectively, such that $0 < \mathcal{H}_t^- < \mathcal{H}_t^+$.

We define the state time derivative as

$$\dot{x}_t = \frac{\beta}{x_t}(\eta_1 d_1 + \eta_2 d_2) + u_t, \tag{17}$$

where u_t represents the tank input and $\beta \in (0,1)$ prevents the tank energy to exceed the maximum value. In particular, $\beta = 1$ if $E_t \le \mathcal{H}_t^+$ and $\beta = 0$ otherwise. We can use $\eta_1, \eta_2 \in [0,1]$ to control how much power is fed from the system to the tank. If there is enough energy available. the tank input is defined such that the tank reserve of energy can be used to compensate actions violating passivity. In particular,

$$u_t(t) = -\frac{1}{x_t}\sum_{i=1}^{3} p_i. \tag{18}$$

We ensure that $x_t > 0 \ \forall \ t$ by adding a lower-limit policy in Section V-C.

A. Passivity analysis

The tank energy dynamics are then given by

$$\dot{\mathcal{H}}_t = x_t \dot{x}_t = \beta(\eta_1 d_1 + \eta_2 d_2) - \sum_{i=1}^{3} p_i. \tag{19}$$

Considering the tank together within the closed loop dynamics, we can write the energy dynamics of the entire system:

$$\dot{\bar{\mathcal{H}}}_{cl} = \dot{\mathcal{H}}_{cl} + \dot{\mathcal{H}}_t = -d_1 - d_2 + \boldsymbol{t}^\top \boldsymbol{w}_{ext} + \sum_{i=1}^{3} p_i + \dot{\mathcal{H}}_t$$
$$= -(1-\beta\eta_1)d_1 - (1-\beta\eta_2)d_2 + \boldsymbol{t}^\top \boldsymbol{w}_{ext} \le \boldsymbol{t}^\top \boldsymbol{w}_{ext}. \tag{20}$$

Thanks to the introduction of the tank, the passivity of the system can be ensured as long as the tank is not fully drained.

V. POWER VALVES AND SAFETY POLICIES

From the previous section it appears that the system passivity, as so stability, can be preserved for every control action as long as the energy tank is not drained to the minimum. Therefore, it is important to design a method to limit the draining of the tank, reducing the non-passive actions and eventually set them to zero when the tank energy reaches its minimum value. This can be done employing the concept to *power valves* introduced in [24] together with some safety policies to regulate their values.

A. Power valves

In order to not only maintain passivity but also in an effort to maximize the chances of executing the given task, we use power valves to control the power flows of passivity-violating tasks individually. We would therefore like to scale the power flows that can lead to a non-passive system such that

$$p_i^* = \boldsymbol{y}_i^\top \boldsymbol{\Gamma}_i \boldsymbol{\omega}_i. \tag{21}$$

where $\boldsymbol{\Gamma}_i = \text{diag}(\gamma_{i,1}, \dots, \gamma_{i,6})$, $i \in \{1,2,3\}$ is a tuning parameter described in the following. This is equivalent to imposing:

$$\boldsymbol{\omega}_1^* = \boldsymbol{w}_{c,tr}^* = \boldsymbol{\Gamma}_1 \boldsymbol{w}_{c,tr} \tag{22a}$$
$$\boldsymbol{\omega}_2^* = \boldsymbol{\Gamma}_2 \bar{\boldsymbol{M}}\hat{\boldsymbol{w}}_{ext} \tag{22b}$$
$$\boldsymbol{\omega}_3^* = \boldsymbol{\Gamma}_3 \boldsymbol{\omega}_3 = \dot{\hat{\boldsymbol{p}}}^* + \boldsymbol{K}_o \hat{\boldsymbol{p}}^*. \tag{22c}$$

It is easy to verify that the new scaled power flows can be obtained by modifying the controller and wrench observer as follows:

$$\begin{aligned} \boldsymbol{w}_c^* &= \boldsymbol{w}_{c,tr}^* + \boldsymbol{w}_{c,imp}^* \\ &= \boldsymbol{\Gamma}_1 \boldsymbol{w}_{c,tr} + \boldsymbol{\Gamma}_2 \bar{\boldsymbol{M}}\hat{\boldsymbol{w}}_{ext} \\ &\quad - (\bar{\boldsymbol{K}}_d \boldsymbol{t} + \bar{\boldsymbol{K}}_p \boldsymbol{e}) - \boldsymbol{C}\boldsymbol{t} - \boldsymbol{w}_g \end{aligned} \tag{23}$$

$$\dot{\hat{\boldsymbol{p}}}^* = \boldsymbol{\Gamma}_3 \boldsymbol{\omega}_3 - \boldsymbol{K}_o \hat{\boldsymbol{p}}^*. \tag{24}$$

B. Valve gain scaling

As shown in (20) the system is passive for any $\boldsymbol{\Gamma}_i$. However, the exact values of $\boldsymbol{\Gamma}_i$ determine the performance in executing the three passivity-violating tasks of external wrench estimation, impedance control, and wrench tracking control. We present different approaches in order to adaptively set the valve gains according to the following goals (in decreasing order of priority):

1) Safe interaction;
2) Correct estimation of external wrenches;
3) Impedance control;
4) Tracking of a reference force.

These goals can be translated into the following valve policies:

1) Limit the total power flow from the tank to the system, i.e., $-\dot{\mathcal{H}}_t \le p_{tot}^+$;
2) Maximize p_3^*, obtained by maximizing $\boldsymbol{\Gamma}_3$;
3) Maximize p_2^*, obtained by maximizing $\boldsymbol{\Gamma}_2$;
4) Maximize p_1^*, obtained by maximizing $\boldsymbol{\Gamma}_1$.

In the following we present three different policies to achieve these goals.

a) Individual Gain Scaling (IGS): The valve gains are scaled according to individually set maximum power limits:

$$\gamma_i = \begin{cases} \frac{p_i^+}{p_i} & \text{if } p_i > p_i^+, \\ 1 & \text{else.} \end{cases} \tag{25}$$

b) Weighted Gain Scaling (WGS): The gains are scaled such that the total power outflow is limited to p_{tot}^+ and the ratios of individual power flows are determined by δ_i:

$$\gamma_i = \begin{cases} \frac{\delta_i p_{tot}^+}{\sum \delta_i p_i} & \text{if } \sum p_i > p_{tot}^+, \\ 1 & \text{else.} \end{cases} \tag{26}$$

c) Sequential Gain Assignment (SGA): Tasks of highest priority are fully admitted until a maximum power limit is reached. The last valve to be actived is scaled so that the maximum allowable power flow is achieved. If the valves are sorted by priorities in descending order (i.e. lower index represents higher priority), then:

$$\gamma_i = \begin{cases} 1 & \text{if } \sum_{j=1}^{i} p_j \le p_{tot}^+, \\ \frac{p_{tot}^+ - \sum_{j=1}^{i-1} p_j}{p_i} & \text{if } \sum_{j=1}^{i} p_j \ge p_{tot}^+, \\ 0 & \text{else.} \end{cases} \tag{27}$$

C. Lower tank limits

In addition to the individual valves, we add a general multiplier α to prevent the tank from draining too close to a lower limit $\mathcal{H}_t^-$. This gain is multiplied with all valve gains, such that $\boldsymbol{\Gamma}_i^* = \alpha \cdot \boldsymbol{\Gamma}_i$. In order to achieve a smooth scaling close to this lower bound we employ a cosine step function between $\mathcal{H}_t^-$ and a threshold ϵ_t:

$$\alpha = \begin{cases} 0 & \text{if } \mathcal{H}_t \leq \mathcal{H}_t^-, \\ \frac{1}{2}\left(1 - \cos\left(\frac{\mathcal{H}_t - \mathcal{H}_t^-}{\epsilon_t}\pi\right)\right) & \text{if } \mathcal{H}_t^- \leq \mathcal{H}_t \leq \mathcal{H}_t^- + \epsilon_t, \\ 1 & \text{else.} \end{cases} \tag{28}$$

VI. EXPERIMENTAL RESULTS

A. Experimental setup

For experiments we use the OMAV presented in [27] and shown in Fig. 1. It is designed with six equally spaced arms with double rotor groups, which can be tilted by servo-motors obtaining omnidirectional thrust vectoring. A rigid arm is attached to the body, pointing along its positive $\boldsymbol{x}_B$-axis. Sensor fusion of an Inertial Measurement Unit (IMU) with an external motion capture system is used for state estimation. A Force-Torque (FT) sensor measures the ground truth force acting at the end-effector. Its measurements $\boldsymbol{f}_{meas}$ are used for comparisons only.

B. Controller implementation

The implementation of the valve policies in a discrete-time controller can lead to strong chattering behavior of the valve gains and the respective power flows. As the valve gains are computed based on the power flows at the previous time step, this can result in alternating exceedingly high and low power flows. In order to mitigate this phenomenon, we apply a first order lowpass filter on $\boldsymbol{\Gamma}_i$ with a cutoff frequency of $2\,\text{Hz}$. While this does not violate passivity, it can lead to an unnecessarily conservative behavior where the control objectives are not fully satisfied because the valves are slowly restored to high values after low ones.

Furthermore, we simplify the valve gain matrices by using five scalars γ_i, resulting in the following multipliers:

$$\begin{aligned} \boldsymbol{\Gamma}_1 &= \text{diag}\left(\gamma_1, \boldsymbol{0}_{1\times 5}\right) \\ \boldsymbol{\Gamma}_2 &= \text{blkdiag}\left(\gamma_{2,lin}\boldsymbol{I}_3, \gamma_{2,ang}\boldsymbol{I}_3\right) \\ \boldsymbol{\Gamma}_3 &= \text{blkdiag}\left(\gamma_{3,lin}\boldsymbol{I}_3, \gamma_{3,ang}\boldsymbol{I}_3\right). \end{aligned} \tag{29}$$

The choice of $\boldsymbol{\Gamma}_1$ leads to a force tracking controller along the body x-axis only, ignoring wrench errors in other directions, which is the goal of the task. We further separate $\boldsymbol{\Gamma}_2$ and $\boldsymbol{\Gamma}_3$ into linear and angular components as their respective power flows have naturally different magnitudes.

C. Comparison of different policies

We evaluate the different policies by pushing with the end-effector against a cart which is able to move freely on a flat ground (see Fig. 1). This is done by first approaching the cart and then activating the wrench tracking controller (WTC). Once the WTC is activated, the impedance controller remains enabled to track a constant position and attitude.
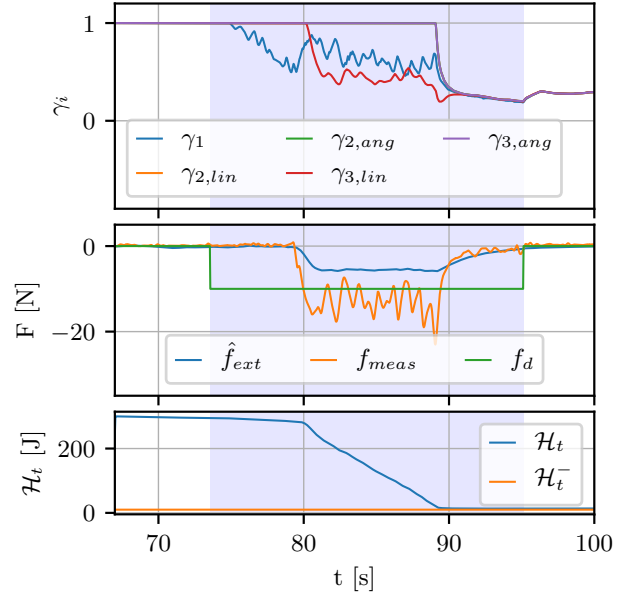

Fig. 3: Valve states, interaction forces, and tank energy for IGS. $\hat{f}_{ext}$ is the estimated interaction force, f_{meas} the FT sensor measurement, and f_d the reference force. The blue shaded area highlights the period during which the WTC is enabled.

For all experiments we use $\eta_1 = \eta_2 = 0.4$ to ensure a high passivity margin, since values around $\eta_i = 1$ can lead to the power in- and outflows balancing each other out.

Individual Gain Scaling: We tuned the five power limits to the following values: $p_1^+ = 1.0$, $p_{2,lin}^+ = 1.0$, $p_{2,ang}^+ = 1.0$, $p_{3,lin}^+ = 30.0$, $p_{3,ang}^+ = 3.0$ [W]. This configuration was chosen following this reasoning: The correct estimation of the external wrench is of highest priority, resulting in the highest allowable power flows in p_3. However, as the power flows created by the linear dynamics are generally about one magnitude larger than the ones created by angular dynamics (given our platform design and dynamic capabilities), we allow $p_{3,lin}$ to be larger than $p_{3,ang}$. The force tracking and impedance power flows are limited to lower values as they can otherwise lead to dangerously large forces.

Figure 3 shows the valve gains and tank energy during one push experiment. Even though the OMAV was at a distance of $0.5\,\text{m}$ upon activation of the WTC, the approach to the (a priori unknown) contact point was performed smoothly due to the wrench tracking power reduction through γ_1. After contact at $t = 80\,\text{s}$, the tank drains quickly through the wrench observer port, leading to a complete draining at which the tracking command is ramped down, stopping the movement. The cart traveled a distance of $0.3\,\text{m}$ in this period. Note that the estimated and measured interaction force differ due to the limited power flow p_3 of the observer.

Weighted Gain Scaling: For WGS we used a maximum allowed power output of $p_{tot}^+ = 90\,\text{N}$ and the following weighting: $\delta_1 = 1.0$, $\delta_2 = 5.0$, $\delta_3 = 5.0$, $\delta_4 = 10.0$, $\delta_5 = 10.0$. Again we assign the highest priorities to the correct wrench estimation and the lowest priority to tracking the reference force. This is reflected in the experimental results shown in Fig. 4. After establishing contact with the cart, the
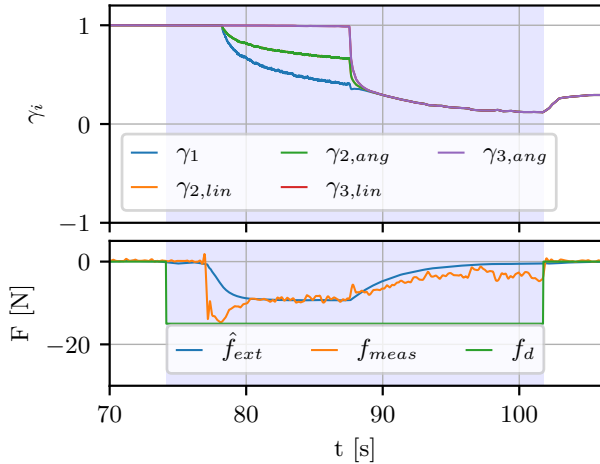
Fig. 4: Valve states and force tracking for WGS. The valves are scaled smoother than in IGS and the interaction force is estimated correctly.

force tracking valve is decreased together with the impedance torque component, until the tank is drained completely and tracking is stopped. The interaction force estimate is more accurate compared to IGS, also resulting in a smoother force tracking. While the valve-scaling behavior of this approach turns out to be not only smoother than in IGS, the tuning of a single maximum power output rather than many individual limits is also more convenient in practice.

Sequential Gain Assignment: The priorities for SGA were set in the following order (from high to low priority): γ_5, γ_4, γ_3, γ_2, γ_1. As the experimental result was similar to the result of WGS, we do not show the related plots for the lack of space. However, this method proved to be very practical, as it depends — once the priority order has been determined — on only one tuning variable (i.e. p_{tot}^+). That way, an interaction task can be attempted with initially low values of p_{tot}^+ in order to guarantee a safe behavior. If the limit is too low for task execution, it can gradually be increased, until the task can be executed.

Discussion: As the three policies have been tuned with the same objectives in mind, the experimental results are similar. However, the tuning procedures are different and turned out to be less tedious for WGS and SGA as compared to IGS.

D. Comparison of IGS and no policy

Lastly, we compare the experiment of pushing a cart over a small obstacle on the ground with employing IGS against employing no policy. For this experiment we assume only a minimal knowledge about the task requirements, which is that a force of 15 N is sufficient to overcome the obstacle. Other parameters such as the state, mass, or friction of the cart are unknown. The maximum allowed power value for the wrench tracking command is set to $p_1^+ = 1.5\,\text{W}$. The results are presented in Fig. 5. Both IGS and no policy are shown, highlighting that the former is able to perform the task while the latter had to be stopped after accelerating too quickly. The different phases are described in the following.

At the start of the experiment, the OMAV is hovering with the end-effector touching the cart (phase 0). In phase 1, the WTC is activated with a constant reference interaction force

of $f_{ref} = 16\,\text{N}$. In phase 2, the cart hits the obstacle and a higher force is needed to overcome it. Once the obstacle has been passed (phase 3), the cart is pushed with limited power, maintaining stability. Eventually, the reference interaction force is never reached due to the power policy. As opposed to IGS, not using a policy leads to a fast increase of $\boldsymbol{w}_{c,tr}$ and consequently a high acceleration of the platform, from which it eventually becomes unstable.

Employing valve gain scaling based on power flows allows to push an unmodeled movable cart, resulting in a safe and robust interaction. Thanks to the formal proof of passivity, the interaction with any passive environment is guaranteed to be stable, i.e., also in the case of a cart with different mass or friction parameters. Additionally, we found that scaling power flows based on their magnitudes rather than on the tank energy is especially suitable for highly dynamic systems such as OMAVs. In fact, we experimentally experienced that the system might diverge when too high power flows limits are set. Limiting these power flows adds another safety layer to the concept of stopping interactions upon a drained tank.
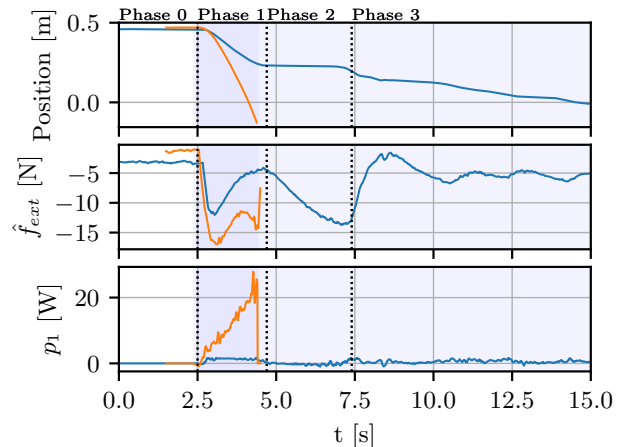

Fig. 5: Pushing a cart over an obstacle. The WTC is activated at $t = 2.5\,\text{s}$. The blue lines represent the outcome with using IGS, the orange line without policies.

VII. CONCLUSIONS

We applied energy tank-based policies for robust interaction with moving environments, where no knowledge nor assumption regarding the environment is required. We observed that especially in interaction with moving objects, the power policies prevent the tank from providing harmful amounts of energy within a short time by limiting the interaction power. The policies are able to reduce the performance of the corresponding control action and ensure a safe dynamic interaction. Scaling the valves according to the described policies proved to be an efficient method to keep power flows within bounds. While the approach ensures safe interaction, it can result in overly conservative control actions which can impede the execution of a task. This could be addressed by adapting the policies online, which we leave to future research.

REFERENCES

[1] A. Ollero, M. Tognon, A. Suarez, D. J. Lee, and A. Franchi, "Past, present, and future of aerial robotic manipulators," *IEEE Trans. on Robotics*, 2021.

[2] M. Hamandi, F. Usai, Q. Sable, N. Staub, M. Tognon, and A. Franchi, "Design of multirotor aerial vehicles: a taxonomy based on input allocation," *accepted, The International Journal of Robotics Research*, vol. 40, no. 8-9, pp. 1015–1044, 2021.

[3] M. Ryll, G. Muscio, F. Pierri, E. Cataldi, G. Antonelli, F. Caccavale, D. Bicego, and A. Franchi, "6D interaction control with aerial robots: The flying end-effector paradigm," in *International Journal of Robotics Research*, vol. 38, no. 9, 2019, pp. 1045–1062.

[4] K. Bodie, M. Tognon, and R. Siegwart, "Dynamic end effector tracking with an omnidirectional parallel aerial manipulator," *IEEE Robotics and Automation Letters*, vol. 6, no. 4, pp. 8165–8172, 2021.

[5] M. Tognon, H. A. Tello Chávez, E. Gasparin, Q. Sablé, D. Bicego, A. Mallet, M. Lany, G. Santi, B. Revaz, J. Cortés, and A. Franchi, "A truly redundant aerial manipulator system with application to push-and-slide inspection in industrial plants," *IEEE Robotics and Automation Letters*, vol. 4, no. 2, pp. 1846–1851, 2019.

[6] A. Suarez, G. Heredia, and A. Ollero, "Physical-virtual impedance control in ultralightweight and compliant dual-arm aerial manipulators," *IEEE Robotics and Automation Letters*, vol. 3, no. 3, pp. 2553–2560, 2018.

[7] X. Meng, Y. He, and J. Han, "Hybrid Force/Motion Control and Implementation of an Aerial Manipulator towards Sustained Contact Operations," *IEEE International Conference on Intelligent Robots and Systems*, pp. 3678–3683, 2019.

[8] K. Bodie, Z. Taylor, M. Kamel, and R. Siegwart, "Towards Efficient Full Pose Omnidirectionality with Overactuated MAVs," pp. 85–95, 2020.

[9] D. Tzoumanikas, F. Graule, Q. Yan, D. Shah, M. Popovic, and S. Leutenegger, "Aerial Manipulation Using Hybrid Force and Position NMPC Applied to Aerial Writing," 2020.

[10] G. Nava, Q. Sablé, M. Tognon, D. Pucci, and A. Franchi, "Direct Force Feedback Control and Online Multi-Task Optimization for Aerial Manipulators," *IEEE Robotics and Automation Letters*, vol. 5, no. 2, pp. 331–338, 2020.

[11] B. Siciliano, L. Sciavicco, L. Villani, and G. Oriolo, *Robotics: Modelling, Planning and Control*. Springer, 2009.

[12] D. Lee, H. Seo, D. Kim, and H. J. Kim, "Aerial Manipulation using Model Predictive Control for Opening a Hinged Door," *Proceedings - IEEE International Conference on Robotics and Automation*, pp. 1237–1242, 2020.

[13] D. Lee, H. Seo, I. Jang, S. J. Lee, and H. J. Kim, "Aerial Manipulator Pushing a Movable Structure Using a DOB-Based Robust Controller," *IEEE Robotics and Automation Letters*, vol. 6, no. 2, pp. 723–730, 2021.

[14] S. Stramigioli, "Energy-Aware Robotics," in *Mathematical Control Theory I*, M. K. Camlibel, A. A. Julius, R. Pasumarthy, and J. M. Scherpen, Eds. Springer International Publishing, 2015, pp. 37–50.

[15] J. J. E. Slotine and W. Li, *Applied nonlinear control*. Prentice Hall, 1991.

[16] E. Nuño, L. Basañez, and R. Ortega, "Passivity-based control for bilateral teleoperation: A tutorial," *Automatica*, vol. 47, no. 3, pp. 485–495, 2011.

[17] N. Chopra and M. W. Spong, *Passivity-Based Control of Multi-Agent Systems*. Berlin, Heidelberg: Springer Berlin Heidelberg, 2006, pp. 107–134.

[18] M. Tognon, C. Gabellieri, L. Pallottino, and A. Franchi, "Aerial co-manipulation with cables: The role of internal force for equilibria, stability, and passivity," *IEEE Robotics and Automation Letters, Special Issue on Aerial Manipulation*, vol. 3, no. 3, pp. 2577 – 2583, 2018.

[19] M. Tognon, R. Alami, and B. Siciliano, "Physical human-robot interaction with a tethered aerial vehicle: Application to a force-based human guiding problem," *IEEE Transactions on Robotics*, vol. 37, no. 3, pp. 723–734, 2021.

[20] V. Duindam and S. Stramigioli, "Port-based asymptotic curve tracking for mechanical systems," *European Journal of Control*, vol. 10, no. 5, pp. 411–420, 2004.

[21] C. Secchi, S. Stramigioli, and C. Fantuzzi, "Position Drift Compensation in Port-Hamiltonian Based Telemanipulation," *2006 IEEE/RSJ International Conference on Intelligent Robots and Systems*, pp. 4211–4216, 2006.

[22] A. Dietrich, X. Wu, K. Bussmann, C. Ott, A. Albusch, and S. Stramigioli, "Passive Hierarchical Impedance Control Via Energy Tanks," *IEEE Robotics and Automation Letters*, vol. 2, no. 2, pp. 522–529, 2017.

[23] R. Rashad, J. B. C. Engelen, and S. Stramigioli, "Energy Tank-Based Wrench / Impedance Control of a Fully-Actuated Hexarotor: A Geometric Port-Hamiltonian Approach," in *International Conference on Robotics and Automation (ICRA)*, no. 3, 2019, pp. 6418–6424.

[24] E. Shahriari, L. Johannsmeier, and S. Haddadin, "Valve-based Virtual Energy Tanks: A Framework to Simultaneously Passify Controls and Embed Control Objectives," in *2018 Annual American Control Conference (ACC)*, 2018, pp. 3634–3641.

[25] K. Bodie, M. Brunner, M. Pantic, S. Walser, P. Pfändler, U. Angst, R. Siegwart, and J. Nieto, "Active Interaction Force Control for Contact-Based Inspection with a Fully Actuated Aerial Vehicle," *IEEE Transactions on Robotics*, vol. 37, no. 3, pp. 709–722, mar 2020.

[26] M. Ryll, G. Muscio, F. Pierri, E. Cataldi, G. Antonelli, F. Caccavale, and A. Franchi, "6D physical interaction with a fully actuated aerial robot," in *2017 IEEE International Conference on Robotics and Automation (ICRA)*. IEEE, 2017, pp. 5190–5195.

[27] K. Bodie, M. Brunner, M. Pantic, S. Walser, P. Pfndler, U. Angst, R. Siegwart, and J. Nieto, "An Omnidirectional Aerial Manipulation Platform for Contact-Based Inspection," in *Proceedings of Robotics: Science and Systems*, 2019.